









RESEARCH ARTICLE | MAY 14 2024

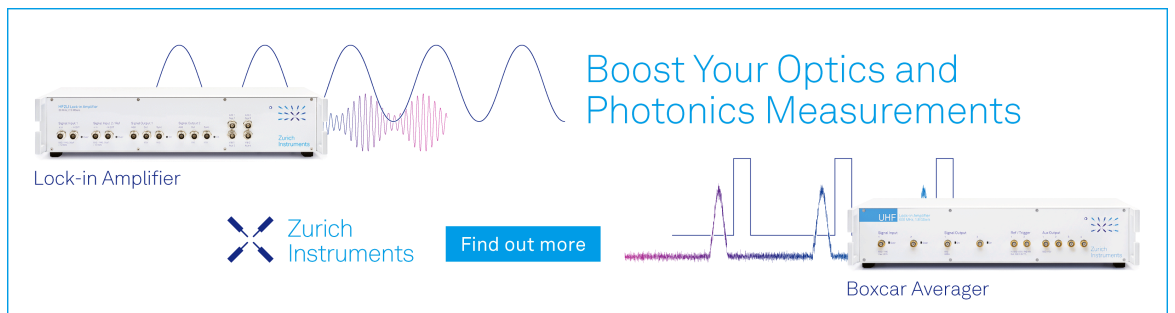
TEMPUS—A microgravity electromagnetic levitation facility for parabolic flights

G. Lohöfer  ; M. Beckers  ; T. Blumberg  ; D. Bräuer   ; S. Schneider  ; T. Volkman  ; A. Meyer 



Rev. Sci. Instrum. 95, 053903 (2024)

<https://doi.org/10.1063/5.0182719>



Boost Your Optics and Photonics Measurements

Lock-in Amplifier

Zurich Instruments

Find out more

Boxcar Averager

TEMPUS—A microgravity electromagnetic levitation facility for parabolic flights

Cite as: Rev. Sci. Instrum. 95, 053903 (2024); doi: 10.1063/5.0182719

Submitted: 20 October 2023 • Accepted: 28 December 2023 •

Published Online: 14 May 2024



View Online



Export Citation



CrossMark

G. Lohöfer,  M. Beckers,  T. Blumberg,  D. Bräuer,^{a)}  S. Schneider,  T. Volkmann,  and A. Meyer 

AFFILIATIONS

Institut für Materialphysik im Weltraum, Deutsches Zentrum für Luft- und Raumfahrt (DLR), 51170 Köln, Germany

^{a)} Author to whom correspondence should be addressed: Dirk.Braeuer@dlr.de

ABSTRACT

During the ~22 s lasting free fall phase in an aircraft flying a parabola, the aboard installed electromagnetic levitation facility “TEMPUS” is used to investigate contactless and undisturbed of gravity induced convection thermophysical properties and microstructure formations of hot and highly reactive metal or semiconductor melts. The completely contactless handling and measurement of a liquid by the levitation technique keeps the melt free of contamination and enables the extension of the accessible sample temperature range far into the undercooled liquid state below the melting point. Additionally, the state of reduced weight during parabolic flights allows us to considerably decrease the strongly disturbing electromagnetic levitation forces acting in ground-based facilities on the suspended liquids. The present paper explains in detail the basic principle and the technical realization of the TEMPUS levitation facility and its attached measurement devices. Furthermore, it presents some typical experiments performed in TEMPUS, which also show the advantages resulting from the combination of reduced weight, electromagnetic levitation, and contactless measurement techniques. The control and data recording, as well as the planning, preparation, and operation of the TEMPUS experiments within the parabolic flight campaign, are another aspect outlined in the following.

© 2024 Author(s). All article content, except where otherwise noted, is licensed under a Creative Commons Attribution (CC BY) license (<https://creativecommons.org/licenses/by/4.0/>). <https://doi.org/10.1063/5.0182719>

I. INTRODUCTION

Thermophysical properties of liquid metals are of central importance for the numerical modeling of solidification, casting, and welding processes and are also relevant for wetting phenomena.¹ Most investigated liquid metals and alloys—often technical multi-component systems with volatile and highly reactive components—have high liquidus temperatures and are prone to evaporation and oxidation problems. Contained in a crucible, the high temperatures and, consequently, the high reaction rates of the most investigated liquid metals with their experimental environment render chemical inert processing a difficult task. Furthermore, since in general the container together with the measurement probes is inserted in a furnace, the thermal expansion of the melt and the crucible and the temperature dependence of the sensors strongly influence the measurement results.²

These problems are bypassed if the handling of the metallic melts as well as the measurement process is performed completely contactless. Furthermore, noninvasive processing offers the additional benefit that, due to the absence of nucleation triggering

crucible walls, liquids can often be undercooled below their solidification temperatures. This effect may considerably enlarge the whole temperature range of the measurement because the maximum temperature of liquid metals is generally strongly limited by their exponentially growing evaporation rate with increasing temperature. Moreover, the lower the temperature of the liquid metal, the more likely it is that a formation of scientifically interesting structures in the melt, like clusters or chemical short range orderings of alloy components, will show up.³

There are several methods for the containerless handling of liquid metals, each with its own technical and application-related assets and drawbacks.^{4,5} Among these, “electromagnetic levitation” (EML) is a notably simple and robust technique for the containerless handling of electrically well-conducting liquids.^{6,7} By applying alternating magnetic fields of high frequency (~350 kHz), electromagnetic levitation stably positions and heats metallic samples without external contact by inductive means only.

For completely noninvasive measurements of the thermophysical properties of liquid metals, like surface tension, viscosity, or electrical resistivity, or for an investigation of microstructure formations

and solidification processes, electromagnetic levitation has to be combined with non-contact measurement devices. These tools are based on optical techniques like pyrometry, which applies Planck's law of radiation for temperature measurements, and videometry,^{8,9} which uses cameras for an analysis of the shape of the levitated droplet. In addition, inductive methods are also applied,¹⁰ which are used for the contactless measurement of the electrical resistivity of a levitated sample and for the detection of its temperature dependent volume change. However, on the ground, all of these methods are more or less severely influenced by the large electromagnetic force fields necessary to suspend the liquid against its weight. They deform the levitated droplet and drive turbulent fluid flows in it. Furthermore, they also strongly heat the droplet, which requires their convective cooling by high-purity noble gases like helium or argon.

These complications are widely removed when electromagnetic levitation and contactless measurements are performed in the largely forceless, so-called "microgravity" (μg) environment. This misleading but adopted expression means that experiments are performed in free fall, either onboard of aircrafts or rockets during parabolic flights or onboard of a spacecraft orbiting around the earth. Under these conditions, the electromagnetic forces can be strongly reduced, and the handling and measurement of the sample can be performed independently by two superposed magnetic fields. To profit from the advantages of microgravity, the "Institute of Materials Physics in Space" of the "German Aerospace Center (DLR)" operates the "TEMPUS" microgravity levitation facility for short time experiments (~ 22 s) during parabolic flights onboard of aircraft (see Fig. 1).

Today's electromagnetic levitation facility, TEMPUS—a German acronym meaning "containerless electromagnetic processing

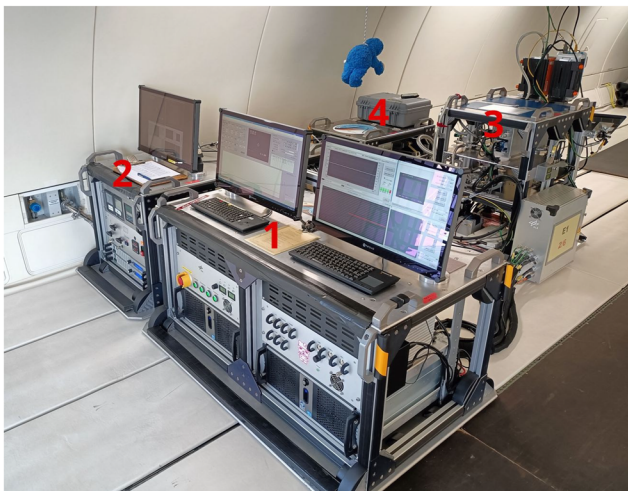


FIG. 1. Image of the TEMPUS levitation facility integrated into the A310 parabolic flight aircraft of Novespace.¹¹ It consists essentially of (1) the "Control-rack" with the experiment control and the data acquisition PCs; (2) the "Generator-rack" containing the power supply, the RF-generators, the gas and vacuum controllers, and the sample transfer control; (3) the "Experiment-rack" with the experiment chamber, the gas system, and the different measurement devices; and (4) the "Supply-rack" with the gas bottles and coil cooling system.

under weightlessness"—dates back to 1986,^{12–14} when its precursor, manufactured by Dornier, was used during the first parabolic flights in 1987 and 1988 in the USA as a test bench for the homonymous "Spacelab" levitation facility. TEMPUS-Spacelab has been applied during two NASA Space Shuttle missions: IML-2 in 1994¹⁵ and MSL-1¹⁶ in 1997. Later on, TEMPUS served during many parabolic flights performed in Europe¹¹ as a breadboard for tests of advanced electromagnetic levitation techniques^{17,18} and of new measurement methods,¹⁹ innovations that are implemented in the electromagnetic levitation facility "ISS-EML," presently on board the "International Space Station."²⁰ Currently, the main attention of the advanced and continuously extended TEMPUS levitation facility is directed to scientific experiments on liquid metals and semiconductors, i.e., to the contactless measurement of their thermophysical properties and to the investigation of their microstructure formations and solidification processes. In the following, we present the levitation principle of TEMPUS, its measurement environment and instruments, the experiment procedure, and some typical experimental methods and results from parabolic flight campaigns.

II. TEMPUS FACILITY

A. Sample positioning and heating system

1. Electromagnetic levitation on ground

Electromagnetic levitation uses a high frequency (≈ 350 kHz) alternating magnetic field $\mathbf{B}(t) = \mathbf{B}_0 \sin(\omega t)$ generated by alternating current carrying coil windings for the containerless lifting and heating of metallic melts. The RF magnetic field induces eddy currents in the sample. These currents heat the sample due to ohmic losses and, in addition, their interaction with the original magnetic field produces Lorentz forces, which point locally in a direction perpendicular to the current and the field (see Fig. 2).

In a first order approximation, the total force exerted by a weakly divergent magnetic field on a tiny metallic sphere is proportional to,^{7,21}

$$\mathbf{F} \propto -\mathbf{B}_0 \cdot \nabla \mathbf{B}_0, \quad (1)$$

and the total power dissipated in it to

$$P \propto \|\mathbf{B}_0\|^2. \quad (2)$$

On the ground, the diverging electromagnetic levitation field is generally used to support metallic samples of about 1 g mass and 5 mm diameter against gravity. On the one hand, electromagnetic levitation provides a technically very simple and stable containerless positioning method for electrically well-conducting materials. On the other hand, however, the high magnetic force field necessary to lift a liquid droplet against gravity often prevents an undisturbed measurement of its thermophysical properties because

- the droplet deforms under the impact of external electromagnetic forces and its weight, which is clearly visible in the image in Fig. 2(b),
- that part of the field that enters the droplet generates turbulent fluid flows in it, which result in a strong stirring of the melt and unsteady oscillations of its shape and,^{22,23}

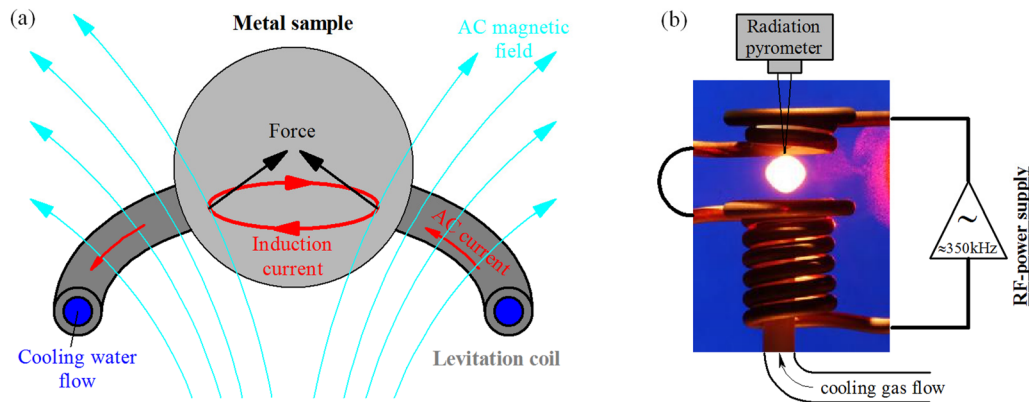


FIG. 2. (a) Principle of electromagnetic levitation. The alternating magnetic levitation field induces eddy currents in the sample which, together with the magnetic field, generate Lorentz forces that support the sample against gravity. This is demonstrated by image (b) of a hot levitated metal droplet enclosed by the alternating current carrying levitation coil on the ground. The coil consists of a water-cooled copper tube. The upper counter windings prevent the lateral escape of the sample. Added is a schematic of the location of the pyrometer for contactless sample temperature measurement and the He/Ar gas flow system for sample cooling. [Figure reproduced from Lohöfer, Rev. Sci. Instrum. **89**, 124709 (2018) with the permission of AIP Publishing LLC.]

- according to Eqs. (1) and (2), lifting and heating of a sample are strongly coupled, so in general, additional cooling has to be established by a stream of chemically inert helium or argon gas blown against the droplet in order to control its temperature.

All of these problems are strongly reduced if electromagnetic levitation is performed under microgravity conditions.

2. Electromagnetic levitation under microgravity

Due to the absence of weight in a microgravity environment, the sole remaining task of the electromagnetic positioning field consists of the containerless confinement of the metallic droplet at a predefined place against external residual forces. For this purpose, the μg electromagnetic levitation facility TEMPUS uses an alternating (≈ 150 kHz) symmetric magnetic quadrupole field produced by two parallel and coaxial circular RF currents of the same strength but in the opposite direction. According to Eq. (1), this so-called “positioning field” repels a displaced weightless metallic sphere to its center between the two coils, where the field strength is weakest

[see Fig. 3(a)] and, therefore, according to Eq. (2), also the inductive heating of the sample.

Moreover, since the residual accelerations on a levitated droplet under microgravity, which have to be compensated by the positioning field, are relatively low ($< 10^{-2}g_0$ during parabolic flights), the remaining magnetic field strength can be decreased to values that are considerably weaker than those necessary to lift the same sample against its weight on the ground, i.e., at $1g_0$. As a result, the disadvantages of electromagnetic levitation in earth-bound laboratories, like shape deformations and surface oscillations generated by the turbulent fluid flow in the levitated melt, are strongly reduced, as video images show. In addition, the necessity to control the sample temperature with an additional convective cooling gas flow no longer exists.

The latter means, however, that for efficient inductive heating and melting of the sample, according to Eq. (2), an additional, widely homogeneous RF (≈ 370 kHz) magnetic dipole field, generated by two parallel and coaxial circular RF currents of the same strength and in the same direction [see Fig. 3(b)], has to be superposed to the quadrupole field. The homogeneity has the additional advantage that, according to Eq. (1), this “heating field,” though it squeezes the

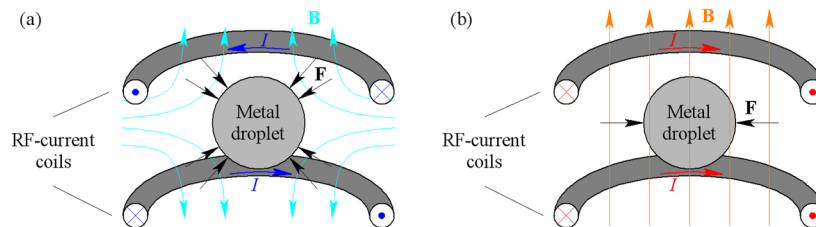


FIG. 3. Sketch of a sample in the center of two circular coils. (a) A RF current in the opposite direction through the upper and lower coils generates a RF magnetic quadrupole field for the positioning of the sample in its center. (b) A RF current in the same direction through the upper and lower coils generates a RF magnetic dipole field for the efficient heating of the sample. [Figure adapted from Lohöfer, Rev. Sci. Instrum. **89**, 124709 (2018) with the permission of AIP Publishing LLC.]

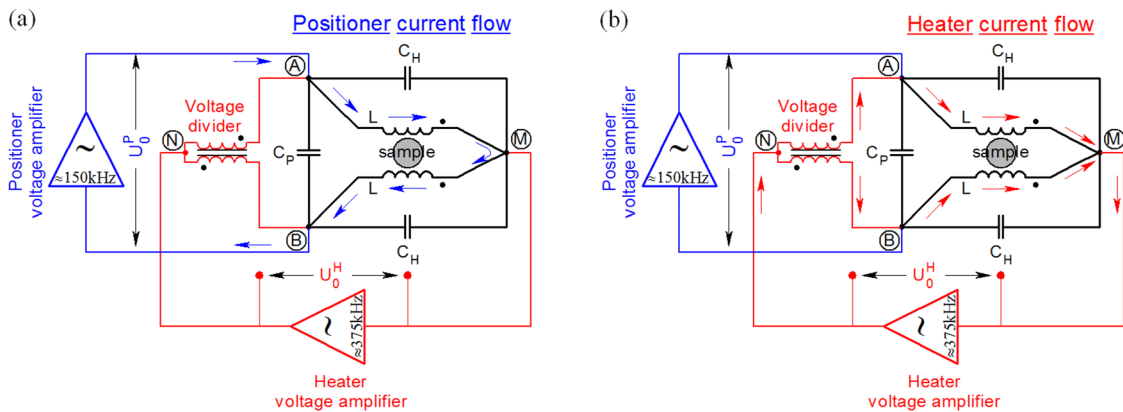


FIG. 4. Two illustrations of the electrical “Supos” circuit, applied in the TEMPUS microgravity electromagnetic levitation facility, showing the different flows of the “positioner” and “heater” currents. The RF current maintained by the positioner voltage amplifier [arrows in (a)] flows in the opposite direction through the upper and lower coil windings, thereby generating a magnetic quadrupole field [see also Fig. 3(a)]. The RF current maintained by the heater voltage amplifier [arrows in (b)] flows in the same direction through the upper and lower coil windings, thereby generating a magnetic dipole field [see also Fig. 3(b)]. [Figure reproduced from Lohöfer, Rev. Sci. Instrum. **89**, 124709 (2018) with the permission of AIP Publishing LLC.]

liquid droplet, does not, however, apply a significant total (center of gravity) force on it, so that positioning and heating of the specimen can almost independently be performed by the dedicated fields.

As already indicated in Fig. 3, both magnetic field shapes can, in principle, be created by the same coils in which the corresponding field generating currents are superposed. The electrical circuit that realizes this so-called “Supos” technique¹⁸ in the TEMPUS μg levitation facility is schematically shown in Fig. 4.

Evidently, due to the symmetry of the currents and the resulting magnetic fields in the “Supos” circuit, which of course presupposes largely identical inductivities L and capacities C_H in the combined resonant circuits of Fig. 4, the positioner current flow does not influence the voltage between the points N and M , and the heater current flow does not influence the voltage between the points A and B . This means that the two amplifiers can be controlled independently of each other.

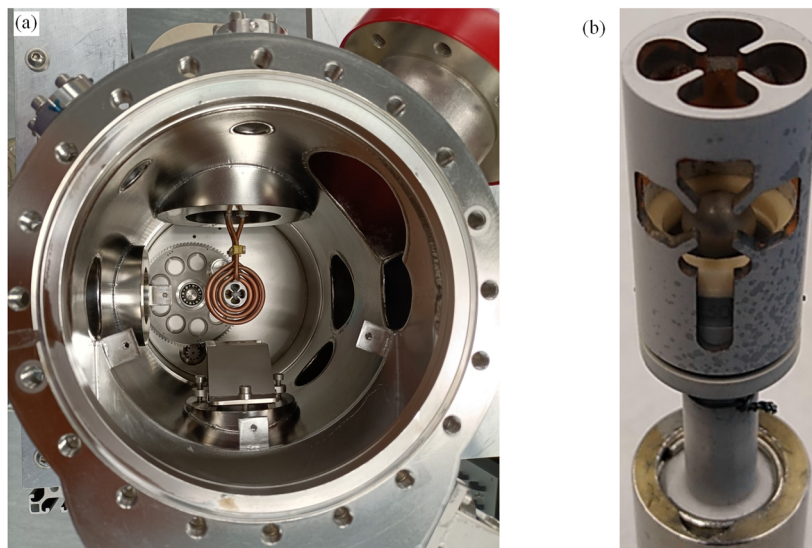


FIG. 5. (a) View into the process and sample chamber of TEMPUS with the internally water cooled levitation coils (copper tubes). The sample chamber mounted below stores up to nine experiment samples, enclosed by a ceramic holder (b), on a rotatable magazine from which they are transferred up into the coil (see also Fig. 6). (b) The cut-outs of the silicon-nitride sample holders allow sufficient visibility of the sample (see Fig. 7 below).

B. Process environment

To guarantee a contamination free sample environment, the levitation coils and the sample handling system are integrated into a stainless steel process chamber [see Fig. 5(a)], connected to a vacuum pump system, and a gas supply allowing experiments in high vacuum or in a clean noble gas atmosphere of helium or argon.

Below the process chamber, the exchangeable sample chamber is mounted. It accommodates up to nine samples of 6–8 mm in diameter to be processed during one flight day. To prevent an inadvertent escape, each sample is enclosed by a SiN ceramic sample holder [see Fig. 5(b)] mounted on a rotatable magazine from which it can be linearly transferred into the center of the coils. Due to the very well-thermally conducting SiN ceramic, there is unobstructed radiative and conductive heat transfer from the sample to the environment and, therefore, no heat buildup inside the holder itself. For a possible additional convective cooling of the sample, the pedestal of the sample holder as well as the transfer rod are hollow to allow a cooling gas flow to the sample from below.

The experimental setup is designed for sample processing in a vacuum or in an inert-gas atmosphere. However, due to the restricted net experiment time of only ~14 s (see, e.g., Fig. 9 below),

experiments on the liquid sample are generally performed in a well-thermally conducting helium gas atmosphere, which allows for quick cooling and solidification of the liquid sample before the end of the low gravity phase.

The technical process gases—argon and helium with impurities of less than 1 ppm—are additionally cleaned by gas purifiers to further reduce the oxygen content and other gas impurities. The whole standard sample processing (see Sec. III B below) happens in a ~10 mbar poorly heat conducting argon atmosphere, which is permanently exchanged by the backing pump in order to remove the dust particles that evaporate from the hot liquid metal sample. This state is maintained during the heating phase. Once the desired maximum sample temperature and, therefore, the start of the experiment is reached, the well heat conducting helium gas is additionally inflated into the process chamber, which allows for the necessary quick cooling and solidification of the liquid sample before the end of the low gravity phase.

Using the convective gas-cooling device, higher cooling rates can be achieved. For this, a helium gas-stream, adjusted by a mass-flow controller, is directed through the hollow pedestal of the sample holder onto the bottom of the levitating sample (see Fig. 6). This method, which is similar to that used on the ground [see Fig. 2(b)],

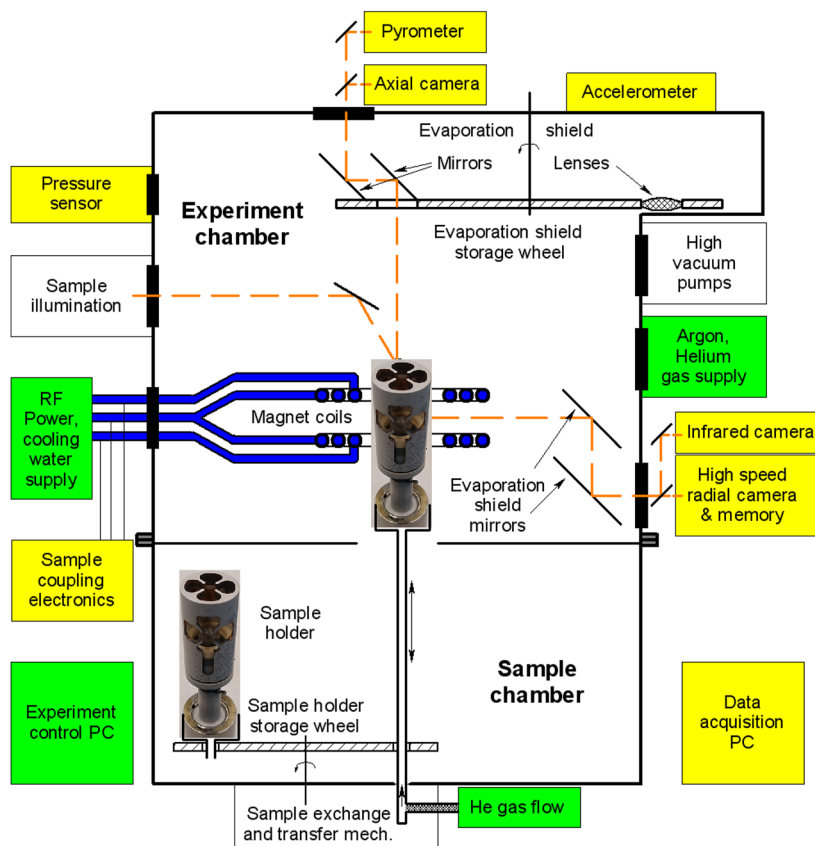


FIG. 6. Functional block diagram of the TEMPUS facility consisting of the experiment chamber, the exchangeable sample chamber, and various command (green) and measurement (yellow) modules, which are connected to the dedicated experiment controller and data acquisition PC.

15 May 2024 07:16:18

results, however, in sample deformations and cannot be combined with all measurement methods (see below).

C. Measurement instruments

To obtain undisturbed scientific data from the levitated sample, various *non-contact* measurement devices are available in TEMPUS.

- A pyrometer is used to measure contactlessly the radiation temperature of the sample.
- Several optical and infrared cameras are used for the observation of the sample from the top and from the side. They look together with the pyrometer through viewports on the top and on the side of the process chamber.
- An inductive measurement device called “Sample Coupling Electronics” (SCE),¹⁹ developed in our institute, allows us to measure contactlessly the electrical resistivity of the sample and its changing shape resulting from (slow) thermal expansions or (quick) surface oscillations.

A schematic overview of the TEMPUS command and measurement modules is given in Fig. 6.

1. Axial camera and pyrometer system

The axial observation system consists of an infrared pyrometer for the contactless radiation temperature measurement of the levitated sample and a camera for its optical inspection, which are integrated into one housing outside of the process chamber. Within this instrument, the visible and infrared light paths are separated and directed to the respective detectors using a beam splitter. The Sensotherm Metis M316 pyrometer is able to measure radiation temperatures between 300 and 2400 °C. The Mikrotron EoSens camera has a pixel size of 14 μm, a resolution of 960 × 960 pixels, and an acquisition rate of 500 frames/s at a gray-scale resolution of 8 bit. By reducing the resolution to 480 × 480 pixels, the frame rate can be extended to 2000 frames/s.

To protect the proper top viewport of the process chamber from metallic vapor and dust deposition stemming from the hot liquid sample and its growing blindness, which impacts the temperature measurement, a wheel with six lenses and three double mirrors is

installed in the optical path inside the vacuum-chamber. The nine optical paths can be exchanged during flight.

2. Radial camera system

For a radial sample observation, various camera configurations can be used, mainly depending on the temperature of the sample during the experiment. For temperatures above ~700 °C, the radiation intensity is high enough that the samples can be observed within the range of visible light. For this, a Phantom v711 camera from Vision Research is used. Its detector has a pixel-size of 20 μm and a gray-scale resolution of 12 bit. Depending on the experiment requirements, the camera operates either in a high-resolution 896 × 800 pixel mode at frame rates of up to 1000 frames/s, which allows the recording of the whole 22 s lasting experiment and is used for thermophysical experiments or slow solidification observation, see e.g., Fig. 7, or in a smaller resolution of 384 × 384 pixel mode with a high frame rate of up to 40 000 frames/s, however, with a recording time of 2 s only, which allows us to observe fast solidification phenomena on the surface of the liquid sample.

These fast events need recording to be triggered either automatically by software detection or manually when the fast sample temperature rise during recalescence is observed. Recording settings and times are predefined before each experiment run. Due to the high data rate, the camera images are stored during the recording in an internal 32GByte ring-buffer, from which they are transferred afterward to a connected non-volatile flash-memory. This needs to be performed during the short time (1 min) between two successive experiment runs (parabolas) and, therefore, limits the maximum recording time.

For sample temperatures below ~700 °C, the radiation intensity from the samples is generally not high enough to observe them within the range of visible light. For this case, an IRCAM Velox~327k infrared camera is used. The camera offers 14 bit images with a 25 μm pixel size. It records up to a frame rate of 1000 frames/s with a resolution of 384 × 384 pixels, but higher frame-rates with reduced image resolutions are also possible. To perform measurements in different temperature ranges, a filter wheel containing various filters is installed in the optical path. Both cameras can be operated in parallel. A silicone window is used as a beam splitter. The combination allows for sample observation over a broad temperature-range.

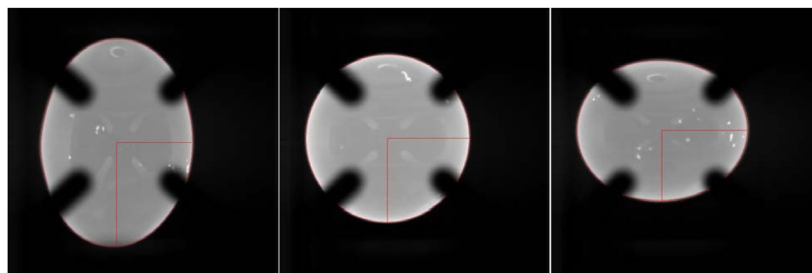


FIG. 7. Sequential images of an oscillating liquid metal sample levitated in TEMPUS and recorded by the radial camera with a slower frame rate. The black rods belong to the sample holder [see Fig. 5(b)]. The artificial red lines stem from the algorithm detecting the droplet edges used for the digital evaluation of sample size and sample oscillations (see Sec. IV below).

3. Inductive measurement device SCE

A benefit of the highly symmetric electrical circuits of TEMPUS discussed earlier and shown in Fig. 4 is the possibility of using the RF magnetic heating field also for inductive measurement of electrical sample properties because

- the heater circuit voltages and currents are not inductively disturbed by the RF magnetic positioner field,
- due to the carefully designed and manufactured coils, the RF magnetic heating (measurement) field is largely homogeneous and, therefore, simple and well defined in the neighborhood of the droplet and,
- the forces of the RF magnetic heating (measurement) field applied to the liquid sample during the inductive measurement process are too low to significantly deform the simple and well-defined spherical shape of the metallic droplet.

According to the diagram in Fig. 4(b), the total electric heating and measurement circuit, which is shown in more detail in the schematic of Fig. 8, consists of two parallel resonant circuits, each of which is composed of one (upper or lower) coil of inductance L , one corresponding (upper or lower) capacitor of capacitance C_H , and the metal sample, which is inductively coupled to both of them.

Since the complex valued sample impedance $\tilde{Z}_S(\omega, a, \rho)$ of the inductively coupled metal is connected in series to the coil impedance \tilde{Z}_L , the total complex valued admittance \tilde{Y}_{tot} , i.e., the inverse total complex impedance, of the heating circuit can be written as

$$\begin{aligned} \tilde{Y}_{tot} &= \frac{2}{\tilde{Z}_C} + \frac{2}{\tilde{Z}_L + \tilde{Z}_S/2} \\ &= \frac{2}{R_C + 1/i\omega C_H} + \frac{2}{R_L + i\omega L + \tilde{Z}_S(\omega, a, \rho)/2}, \end{aligned} \quad (3)$$

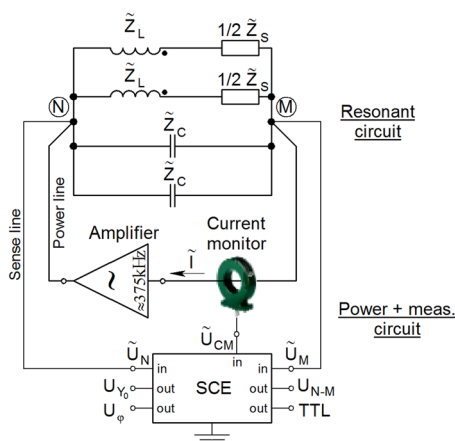


FIG. 8. Schematic wiring diagram of the inductive measurement system of TEMPUS. It consists of the resonant heating circuit shown in Fig. 4(b) and the measurement setup with the inductive current monitor and the measurement electronics “SCE.” The SCE processes the RF input voltages from both ends of the resonant circuit and the signal voltage from the current monitor. [Figure reproduced from Lohöfer, Rev. Sci. Instrum. **89**, 124709 (2018) with the permission of AIP Publishing LLC.]

where R_C and R_L denote the resistances of the capacitor and coil, respectively, and ω is the angular frequency of the magnetic heating field. According to Ref. 24, the impedance $\tilde{Z}_S(\omega, a, \rho)$ of a spherical sample depends on the frequency $f = \omega/2\pi$ of the heating (measurement) field, the radius a , and the electrical resistivity ρ of the processed material.

The measurement task taken by the so-called “Sample Coupling Electronics” (SCE)¹⁹ consists essentially of the determination of

$$\tilde{Y}_{tot} := \tilde{I}/\tilde{U} = I_0/U_0 e^{-i\phi}, \quad (4)$$

i.e., in the measurement of I_0 , U_0 , and $\phi = \phi_U - \phi_I$, which are the amplitude of the alternating current through the total heating circuit, the amplitude of the alternating voltage-drop across the total heating circuit, and the phase shift between both, respectively. With the knowledge of the circuit parameters L , C_H , R_L , and R_C from a calibration experiment without a sample, these measurement results allow us to determine, via Eqs. (3) and (4), the sample impedance $\tilde{Z}_S(\omega, a, \rho)$.

Due to the high 16 bit resolution of the adjacent data acquisition unit, which monitors the output data of the SCE, $\tilde{Z}_S(\omega, a, \rho)$ can be used to very precisely determine the temperature T dependent radius $a(T)$ and the temperature dependent electrical resistivity $\rho(T)$ of the inductively coupled sample (see Sec. IV B below). Moreover, due to its high 400 Hz acquisition rate, the SCE data allow also for very precise detection of the surface oscillations of the liquid sample used for the “Oscillating Drop” measurement method.

D. Experiment control and data recording

The short net experiment time of ~ 14 s, see, e.g., Fig. 9 below, requires a detailed predefined automatic process control that allows, however, at any time, a manual intervention by the TEMPUS operators. Therefore, prior to each parabola (experiment cycle), a control file is loaded into the experiment control computer. It determines, in dependence of the experiment time or the sample temperature, the forces and heating exerted on the sample by setting the generator (amplifier) voltages applied on the respective circuits, as well as the (cooling) gas atmosphere in the process chamber. Additionally, it defines the performance of the measurement instruments by configuring the pyrometer (sample emissivity) and the cameras (frame rate and resolution). Furthermore, it also records and stores, at a rate of 100 Hz, the pyrometer temperature data as well as the various housekeeping data, like chamber pressure, generator voltages, cooling water temperatures, etc. The second so-called video computer runs the image recording software for the axial camera system and for the live preview of the high speed camera or, alternatively, the infrared camera.

During the experiment, the software on the control computer automatically starts and stops recording the data and camera images depending on the acceleration data from the accelerometer. The data are displayed to the operator and recorded on solid-state drives. Recorded data are easily accessible immediately after the parabola for a quick interim analysis.

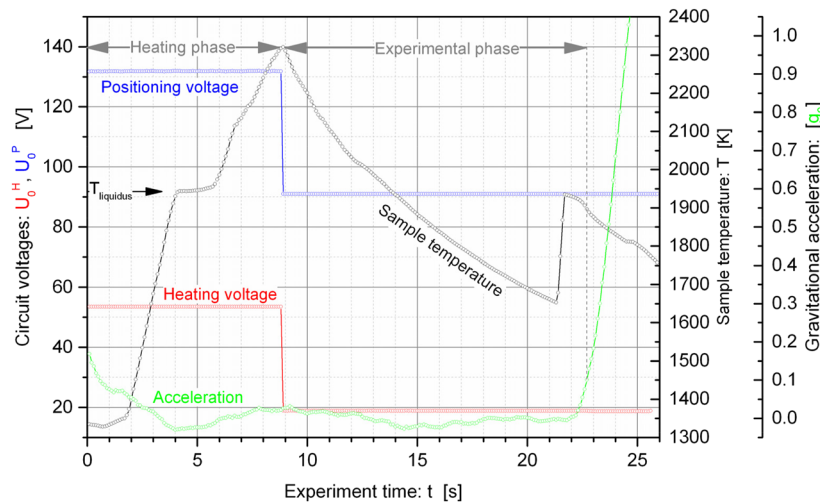


FIG. 9. Example for a typical experiment cycle in the TEMPUS levitation facility during the ~22 s lasting low gravity phase of a flown parabola. Plotted are the measured gravitational acceleration (green), the externally controlled voltages of the positioning (blue) and heating (red) circuits (see Fig. 4), respectively, as well as the resulting temperature of the levitated sample (black). The experiments are performed after the heating and positioning voltages have been reduced. In this phase of the lowest external impact, the liquid sample cools (in this example below its melting temperature) and solidifies, where, due to the sudden release of heat from fusion, its temperature jumps to its melting temperature (recalcescence) and continues its cooling in the solid state.

III. TEMPUS OPERATIONS

A. Campaign preparation

The campaign preparation starts after the evaluation and selection of the received scientific experiment proposals, which typically comprise 12–15 different experiments with 15–20 different samples. Due to the short time and, therefore, difficult experiment conduction, an extensive ground support program is performed at DLR. A timeline is created, and due dates are defined for the collection of test and flight samples and their spares, which have to be delivered by the responsible “Principal Investigator” (PI) of each experiment. Prior to the main experiment, measurements on the test samples are performed on the ground for an investigation of their coupling to the magnetic fields and for a determination of their spectral emissivities. Historical record sheets are used to track the history of each sample from its creation, handover, integration into the sample chamber, in-flight processing, and post-flight treatment.

The parabolic flight experiments are planned together with the responsible PI. For each experiment and sample, a list of flight procedures is created, which contains all the relevant information for the successful conduction of each experiment run during a parabola and forms the basis for the experiment control file. They contain, for example, the initial atmosphere, the intended temperature range, the preheating temperature, the settings for the measurement instruments, the excitement of sample oscillations, the intended cooling methods and their details, the liquidus temperature and spectral emissivity of the sample, etc. With this information, a draft flight plan is created and subsequently optimized with the ongoing experiment planning. The experiments are grouped by their scientific scope, hardware usage, and operational boundary conditions.

Before the flight, the experiment samples are integrated on the ground into their dedicated holders according to the PI’s requirements. Immediately before the flight day, the samples are carefully integrated into their dedicated magazine positions in the sample chamber. The latter is attached to the experiment chamber of the TEMPUS facility and flooded with pure inert argon gas to prevent contamination. This process is documented within the sample integration protocol.

B. Parabolic flight operation

In general, TEMPUS joins one parabolic flight campaign each year. The campaigns are usually operated by Novespace with an Airbus A310 aircraft from the airport in Bordeaux.¹¹ Every campaign has three to four flight days, with 31 flown parabolas per day. The flights are preceded by a preparation week in which the facility racks are installed in the aircraft, cabled, and checked.

The parabolas flown on one day are generally divided into six blocks of 5 to 6 parabolas, with breaks of 3–8 minutes in between. The breaks are used by the four TEMPUS operators for sample exchange, sample preheating, planned readjustments of the experiment settings, or last minute changes depending on the interim analysis of the preceding experiment result, and for the settling of accidental occurrences. The experiments are supervised and governed by a fifth operator and the PI, who proposed the current experiment on the levitated sample. The typical experiment procedure in the TEMPUS facility during one parabola is shown in Fig. 9.

1. Before the beginning of the low gravitational acceleration, due to the limited experiment time, the sample, sitting on the

pedestal of its holder, is already preheated in the solid state in a low pressure atmosphere of thermally poor conducting argon gas.

2. After the onset of the steady low gravity phase, the data acquisition is automatically triggered, and the preheated solid sample is moved on the holder pedestal into the center of the coils, where it is contactlessly positioned by the magnetic positioning field with maximal strength. Once the sample levitates stably, the automatic process control is started. It takes over further process control and raises the magnetic heating field. During this “heating phase,” see Fig. 9, the specimen is melted and overheated over its liquidus temperature.
3. Having reached the predefined maximum sample temperature, the major cooling or “experimental phase,” see Fig. 9, is automatically started by reducing the magnetic heating field to its technically lowest possible value and by reducing the magnetic positioning field to a value that still keeps the droplet safely in place against possible external residual accelerations. In this phase of the lowest external impact on the liquid droplet, the experiments take place after the strong external disturbances in the liquid during the heating phase decayed within the first few seconds. The predefined experiment run is conducted automatically. Furthermore, during this phase, the cooling of the liquid sample is increased by inflating thermally well conducting helium gas into the process chamber in order to obtain a solidified sample at its end.
4. The beginning high acceleration phase deposits the solidified sample again on its holder pedestal and stops automatically the data acquisition and process control. In the following break, the gas pump removes the high thermally conducting helium gas atmosphere from the process chamber. Low thermally conducting argon gas is filled in, and the facility is brought into the experimental configuration for the next parabola.

After the flight, the samples are exchanged, and the facility is prepared for the next flight day. Finally, all monitored raw data are preprocessed for further use by the experimenter (PI) and stored in a database.

IV. EXPERIMENTAL METHODS

A. Viscosity and surface tension

To measure contactlessly the surface tension and viscosity of a liquid metal, the so-called “Oscillating Drop Method” is used.⁸ For this, the levitated liquid droplet is squeezed by a short-time pulse of the levitation force. It is apparent that the following damped oscillation of the droplet surface around its static equilibrium shape is governed by the surface tension of the liquid, which acts as a restoring force, and by the viscous shear flow in the liquid, which acts as a damping mechanism. To determine these two thermophysical properties, the movement of the surface has to first be detected non-invasively by optical (camera), see Fig. 7, or electrical inductive (SCE) means and evaluated with regard to its oscillation frequency ω and damping time τ .²⁵ Under the condition of only marginal external forces acting on the oscillating but non-rotating droplet, which means that its equilibrium shape is spherical, as this is the case in TEMPUS in low gravity, and of only small oscillation amplitudes $|\varepsilon(\mathbf{x}_S)| \ll 1$, the time dependence of the distance from the center of the equilibrium sphere of radius a to any point \mathbf{x}_S on its surface, as schematically shown in Fig. 10 (left), can be described by²⁶

$$r(t, \mathbf{x}_S) = a \left(1 + \varepsilon(\mathbf{x}_S) \cdot e^{-t/\tau} \sin \omega t \right), \quad (5)$$

where $\varepsilon(\mathbf{x}_S)$ describes the surface shape of the lowest damped oscillation mode expanded in spherical harmonics and ω and τ the corresponding frequency and damping time, respectively.

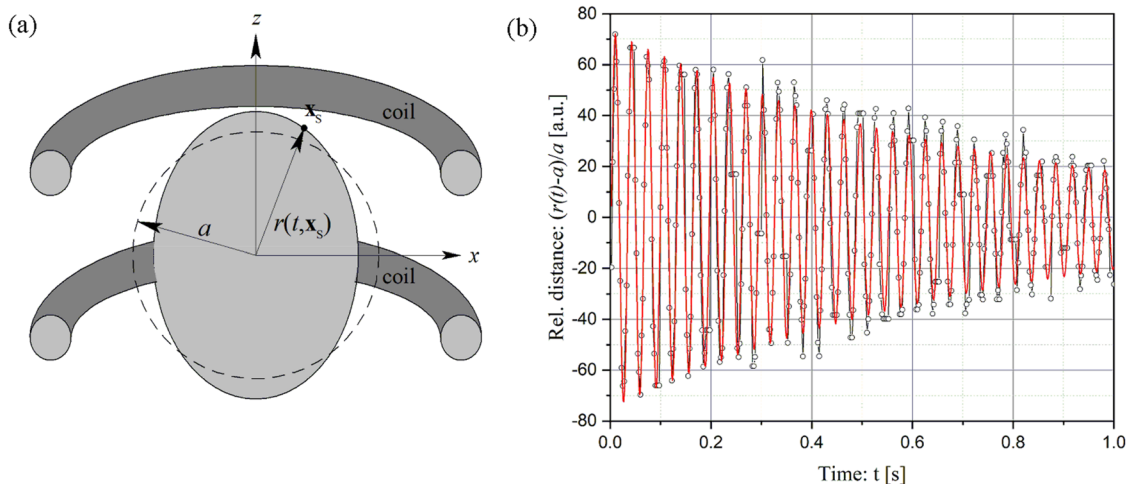


FIG. 10. (a) Schematic cut through a freely levitated liquid droplet oscillating in weightlessness around its equilibrium spherical shape of radius a . (b) Example for the measured time dependent radius change $(r(t) - a)/a$ of this oscillating metal droplet. The measurement points (black circles) are plotted together with a fitted exponentially decaying sine curve (red line), which yields ω and τ .

Finally, these measurement quantities have to be associated via a reasonable physical theory^{26,27} with the surface tension coefficient γ and the viscosity coefficient η ,

$$\omega^2 = \frac{32\pi}{3} \frac{\gamma}{M} \quad \text{and} \quad \frac{1}{\tau} = \frac{20\pi a}{3} \frac{\eta}{M}, \quad (6)$$

where M denotes the sample mass. Due to the temperature drop during the experiment (see Fig. 9), the measured oscillation period $2\pi/\omega$ as well as the damping time τ should be sufficiently short so that the attribution of one value T from this temperature range to $\gamma(T)$ and $\eta(T)$ is still reasonable.

B. Electrical resistivity and density

The real and imaginary parts of the complex valued impedance \tilde{Z}_S of the levitated spherical sample, measured inductively by the SCE during the experimental phase (see earlier), can be used to determine its electrical resistivity ρ and radius a . In the homogeneous magnetic heating field of TEMPUS, the functional dependence between $\tilde{Z}_S(\omega, a, \rho)$ and the sample specific properties a and ρ reads¹⁹

$$\tilde{Z}_S(\omega, a, \rho) = cc \cdot \omega \cdot a^3 \left[\frac{1}{q} - \frac{1}{q^2} + i \left(\frac{1}{q} - \frac{2}{3} \right) \right], \quad (7)$$

under the condition, which is satisfied for the TEMPUS heating circuit, that

$$q(\omega, a, \rho) := \frac{a}{\delta} = a \sqrt{\frac{\mu_0 \omega}{2\rho}} \geq 3, \quad (8)$$

where the dimensionless quantity $q(\omega, a, \rho)$ denotes the relation between the sample radius a and the skin depth $\delta := \sqrt{2\rho/(\mu_0\omega)}$ with vacuum permeability μ_0 . The ‘‘coil constant’’ cc in Eq. (7) is a purely coil geometry dependent factor and describes the interaction of the particular TEMPUS heating coil with the (spherical) sample in its center. The relations in Eqs. (3), (4), (7), and (8) allow to determine independently from each other the electrical resistivity ρ and the radius a of the processed material from a measurement of the real and imaginary parts of the sample impedance \tilde{Z}_S , after a calibration run with a metallic sample of known properties has revealed the coil constant cc . A more detailed description can be found in Ref. 19. An example of a temperature dependent electrical resistivity measured in TEMPUS is shown in Fig. 11.

The temperature dependent density can also be measured using optical methods. For this, the radial camera records video images from the sample, which have to be processed in a second step by an edge detection algorithm (see, e.g., Fig. 7) in order to obtain the temperature dependent sample size. The latter makes the optical method, however, more laborious.

C. Solidification

Containerless processing is a powerful tool to investigate rapid solidification processes and related non-equilibrium effects in undercooled melts.^{30,31} Levitation of liquid droplets combined with high-speed video imaging enables the analysis of the morphology of the solidification front and the measurement of the growth velocity of the solid–liquid interface.^{32,33} During the solidification

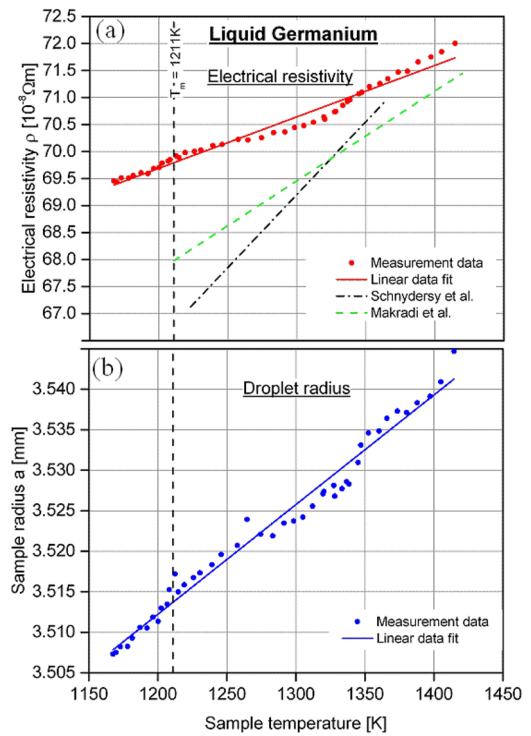


FIG. 11. (a) Plot of the temperature dependent electrical resistivity of liquid germanium measured inductively in TEMPUS using the SCE (dots) compared with data measured by different methods (scattered lines).^{28,29} (b) Plot of the temperature dependent droplet radius change (thermal expansion) resulting from the SCE data. Due to the contactless measurement method, the data extend into the undercooled liquid state below the melting temperature of 1211 K (Experiment Pl: Y. Luo, Uni Göttingen, 2017).

of undercooled melts, the temperature is raised up to the melting point (recalescence) due to the released heat of fusion, as shown by the temperature-time profile in Fig. 9. Due to the sharp temperature jump at the solidification front, its propagation through the liquid sample can be tracked by its thermal field. A sequence of high-speed video images recorded by the radial camera of TEMPUS during the recalescence of an undercooled Fe_{99.3}C_{0.2}Si_{0.5} steel sample is shown in Fig. 12.

The steep temperature gradient at the solid–liquid interface causes a sharp contrast in brightness, which enables monitoring the shape of the solidification front and its propagation when the front intersects the surface of the droplet. The fourfold symmetry visible on the surface originates from dendrite branches growing perpendicular to each other, as expected for cubic metals whose dendrites are growing preferentially along the (100) crystallographic directions.³⁴ Accordingly, the envelope of the dendritic grain exhibits the shape of an octahedron, whose apexes correspond to the tips of the primary dendrite stems and whose edges are formed by side branches growing perpendicular to the primary stems. Using ray tracing software,³⁵ the surface contour of the solidification front has been modeled, thus enabling the reconstruction of the pathway of the three-dimensional front through the droplet as shown in Fig. 12(b).

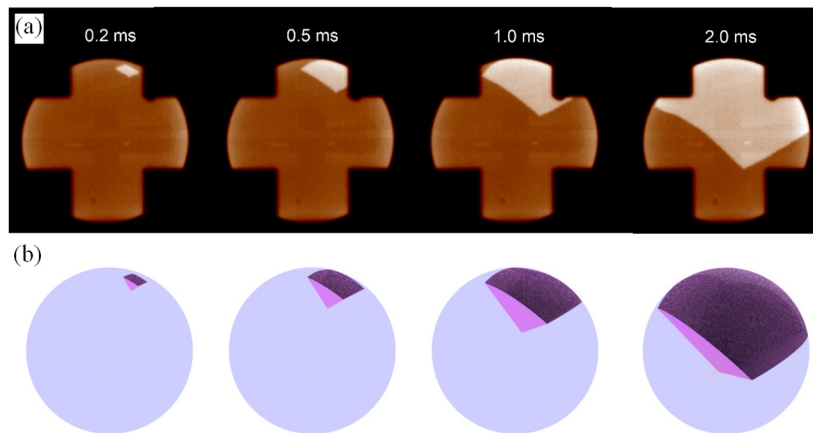


FIG. 12. (a) Sequence of high-speed video images recorded with the radial camera at 30 000 frames/s during rapid solidification of a $\text{Fe}_{99.3}\text{C}_{0.2}\text{Si}_{0.5}$ alloy melt at an undercooling of 70 K in comparison to (b) the modeled surface morphology of the solidification front.

From the images in Fig. 12, it becomes obvious that the precision of modeling the surface contour and, therefore, the growth velocity measurement depends on the knowledge of the exact shape of the droplet, which is a non-oscillating, ideal sphere when levitated under microgravity conditions. Furthermore, this condition is also necessary to avoid the influence of melt convection on growth kinetics. Hence, electromagnetic levitation in a reduced gravity environment such as the utilization of TEMPUS during parabolic flights allows studying solidification processes under (nearly) diffusive conditions.

V. SUMMARY

For widely undisturbed physical investigations of hot or highly reactive metal or semiconductor melts, it is very favorable to use containerless handling techniques in weightlessness in combination with contactless measurement methods. These conditions can be realized for ~ 22 s in the TEMPUS facility aboard an aircraft flying a parabola. For the containerless handling of electrically conducting liquids in a vacuum or a clean noble gas environment, as well as for their heating and melting, TEMPUS applies the notably simple and robust electromagnetic levitation technique. For the completely contactless measurements of thermophysical properties of liquids, like surface tension, viscosity, electrical resistivity, or thermal expansion, or for an investigation of microstructure formations and solidification processes, TEMPUS provides additionally non-contact measurement devices like a pyrometer, an inductive measurement tool, and different types of cameras.

TEMPUS is a multi-user facility, providing for each flight day up to nine different experiment samples. Performed by Novespace¹¹ with an Airbus A310 aircraft based on the airport of Bordeaux, France, each flight day comprises 31 parabolas and, therefore, for the nine samples, 31 experiments on high (<2400 °C) and low (>300 °C) temperature metallic or doped semiconductor melts. During a flown parabola, TEMPUS provides, within a net experiment time of ~ 14 s, a residual acceleration on the levitated samples of $<10^{-2}g_0$. If these conditions are sufficient for a successful experiment performance,

TEMPUS offers several convenient advantages: there is at least one parabolic flight campaign with TEMPUS available each year, the experiment preparation time is short and uncomplicated, the experimenter (PI) can supervise and intervene in the experiment process on board of the airplane, he can partly include his own experiment devices in the TEMPUS facility and, finally, he obtains the measurement data shortly after the end of the campaign.

The present paper explains in detail the basic principles and the technical realization of the TEMPUS facility, i.e., its sample positioning and heating system, its process environment, the available measurement instruments, the experiment procedure, and the typically applied experiment methods.

ACKNOWLEDGMENTS

The authors gratefully acknowledge the permanent administrative support of the TEMPUS project by the DLR Space Administration.

AUTHOR DECLARATIONS

Conflict of Interest

The authors have no conflicts to disclose.

Author Contributions

G. Lohöfer: Writing – original draft (equal); Writing – review & editing (equal). **M. Beckers:** Writing – review & editing (equal). **T. Blumberg:** Writing – review & editing (supporting). **D. Bräuer:** Writing – review & editing (equal). **S. Schneider:** Writing – review & editing (equal). **T. Volkmann:** Writing – review & editing (equal). **A. Meyer:** Writing – review & editing (equal).

DATA AVAILABILITY

The data that supports the findings of this study are available within the article.

REFERENCES

- ¹T. Iida and R. I. L. Guthrie, *The Physical Properties of Liquid Metals* (Clarendon Press, Oxford, 1988).
- ²B. Delley, H. U. Künzi, and H.-J. Güntherodt, "Contactless resistivity measurements on liquid metals," *J. Phys. E: Sci. Instrum.* **13**, 661–664 (1980).
- ³Y. Luo, B. Damaschke, G. Lohöfer, and K. Samwer, "Thermophysical properties of a Si₅₀Ge₅₀ melt measured on board the international space station," *npj Microgravity* **6**, 10 (2020).
- ⁴P. Heintzmann, F. Yang, S. Schneider, G. Lohöfer, and A. Meyer, "Viscosity measurements of metallic melts using the oscillating drop technique," *Appl. Phys. Lett.* **108**, 241908 (2016).
- ⁵I. Jonas, W. Hembree, F. Yang, R. Busch, and A. Meyer, "Industrial grade versus scientific pure: Influence on melt properties," *Appl. Phys. Lett.* **112**, 171902 (2018).
- ⁶E. C. Okress, D. M. Wroughton, G. Comenetz, P. H. Brace, and J. C. R. Kelly, "Electromagnetic levitation of solid and molten metals," *J. Appl. Phys.* **23**, 545–552 (1952).
- ⁷G. Lohöfer, "Theory of an electromagnetically levitated metal sphere I: Absorbed power," *SIAM J. Appl. Math.* **49**, 567–581 (1989).
- ⁸J. Brillo, G. Lohöfer, F. Schmidt-Hohagen, S. Schneider, and I. Egly, "Thermophysical property measurements of liquid metals by electromagnetic levitation," *Int. J. Mater. Prod. Technol.* **26**, 247–273 (2006).
- ⁹I. Egly, G. Lohöfer, and D. Matson, "EML processing measurement techniques," *High Temp. Mater. Processes* **27**, 389–399 (2008).
- ¹⁰G. Lohöfer and G. Pottlacher, "Inductive measurement of thermophysical properties of electromagnetically levitated metallic melts," *High Temp. - High Pressures* **40**, 237–248 (2011).
- ¹¹See www.airzerog.com for more information about AirZeroG, weightless with Novespace.
- ¹²J. Piller, R. Knauf, G. Lohöfer, D. M. Herlach, and P. Preu, "Electromagnetic positioning and inductive heating under micro-g," in *Proceeding of the 6th European Symposium on Material Sciences Under Microgravity Conditions, Bordeaux, France, 2-5 December 1986*, (European Space Agency, 1987), pp. 437–443, ESA SP-256.
- ¹³G. Lohöfer, P. Neuhaus, and I. Egly, "TEMPUS - a facility for measuring the thermophysical properties of undercooled liquid metals," *High Temp. - High Pressures* **23**, 333–342 (1991).
- ¹⁴J. H. Zong, J. Szekely, and G. Lohöfer, "Calculations and experiments concerning lifting force and power in TEMPUS," *Acta Astronaut.* **29**, 371–378 (1993).
- ¹⁵Tempus Team, "Containerless processing in space: Recent results," in *Materials and Fluids Under Low Gravity, Lecture Notes in Physics*, edited by L. Ratke, H. Walter, and B. Feuerbacher (Springer, Berlin, 1996), Vol. 464, pp. 233–252.
- ¹⁶*Solidification 1999: Proceedings of the symposium*: "TEMPUS-Spacelab processing of metallic melts," edited by W. H. Hofmeister, J. R. Rogers, N. B. Singh, S. P. Marsh, and P. W. Vorhees (The Minerals, Metals & Materials Society, Warrendale, 1999).
- ¹⁷G. Lohöfer and J. Piller, "The new ISS electromagnetic levitation facility: MSL-EML," in *Proceedings of the 40th AIAA Aerospace Sciences Meeting & Exhibit* (American Institute of Aeronautics and Astronautics, Reno, USA, 2002), Vol. 14, pp. AIAA 2002-0764.
- ¹⁸G. Lohöfer, German Patent No. 3836239 (08 August 1991), and United States Patent No. 4,993,043 (12 February 1991).
- ¹⁹G. Lohöfer, "High-resolution inductive measurement of electrical resistivity and density of electromagnetically levitated liquid metal droplets," *Rev. Sci. Instrum.* **89**, 124709 (2018).
- ²⁰A. Seidel, W. Soellner, and C. Stenzel, "EML—An electromagnetic levitator for the international space station," *J. Phys.: Conf. Ser.* **327**, 012057 (2011).
- ²¹P. R. Rony, "The electromagnetic levitation of metals," in *Proc. Trans. Vacuum Met. Conf. 1964*, edited by M. A. Cocca (Am. Vacuum Society, Boston, MA, 1965), pp. 55–135.
- ²²V. Bojarevics and K. Pericleous, "Modelling electromagnetically levitated liquid droplet oscillations," *ISIJ Int.* **43**, 890–898 (2003).
- ²³R. W. Hyers, "Fluid flow effects in levitated droplets," *Meas. Sci. Technol.* **16**, 394–401 (2005).
- ²⁴G. Lohöfer, "Magnetization and impedance of an inductively coupled metal sphere," *Int. J. Eng. Sci.* **32**, 107–117 (1994).
- ²⁵M. Beckers, M. Engelhardt, and S. Schneider, "Contactless measurement of temperature dependent viscosity and surface tension of liquid Al_{69.1}Cu_{12.8}Ag_{18.1} eutectic alloy under microgravity conditions using the oscillating-drop-method," *High Temp. - High Pressures* **50**, 167–184 (2021).
- ²⁶S. Chandrasekhar, *Hydrodynamic and Hydromagnetic Stability* (Dover Publications, New York, 1981).
- ²⁷G. Lohöfer, "Viscosity measurement by the oscillating drop method: The case of strongly damped oscillations," *Int. J. Thermophys.* **41**, 30 (2020).
- ²⁸H. S. Schnyders and J. B. V. Zytveld, "Electrical resistivity and thermopower of liquid Ge and Si," *J. Phys.: Condens. Matter* **8**, 10875–10883 (1996).
- ²⁹A. Makradi, J. G. Gasser, J. Hugel, A. Yazı, and M. Bestandji, "Experimental electrical resistivity and thermopower of molten germanium interpreted with muffin-tin potential calculations," *J. Phys.: Condens. Matter* **11**, 671–686 (1999).
- ³⁰D. M. Herlach, "Non-equilibrium solidification of undercooled metallic melts," *Mater. Sci. Eng.* **12**, 177–272 (1994).
- ³¹D. M. Herlach, P. K. Galenko, and D. Holland-Moritz, *Metastable Solids from Undercooled Melts* (Elsevier, Amsterdam, 2007).
- ³²D. M. Matson, "The measurement of dendrite tip propagation velocity during growth into undercooled metallic melts," in *Solidification 1998*, edited by S. P. Marsh, J. A. Dantzig, R. Trivedi, W. Hofmeister, M. G. Chu, E. J. Laverna, and J.-H. Chun (The Minerals, Metals & Materials Society, 1998), pp. 233–244.
- ³³T. Volkmann, "Measurement of crystal growth velocities in undercooled melts of metals," in *Solidification of Containerless Undercooled Melts*, edited by D. M. Herlach and D. M. Matson (Wiley, Weinheim, Germany, 2011), pp. 239–259.
- ³⁴B. Chalmers, *Principles of Solidification*, 2nd ed. (Wiley, New York, 1967), pp. 103–125.
- ³⁵See <http://www.povray.org/> for more information about Persistence of vision^(TM) raytracer, 2004.